Asymptotic-Preserving schemes for kinetic–fluid modeling of disperse two-phase flows

Thierry Goudon[*†] Shi Jin[‡] Jian-Guo Liu[§] Bokai Yan[‡]

May 11, 2011

Abstract

We consider a system coupling the incompressible Navier–Stokes equations to the Vlasov–Fokker–Planck equation. Such a problem arises in the description of particulate flows. We design a numerical scheme to simulate the behavior of the system. This scheme is asymptotic-preserving, thus efficient in both the kinetic and hydrodynamic regimes. It has a numerical stability condition controlled by the non-stiff convection operator, with an implicit treatment of the stiff drag term and the Fokker-Planck operator. Yet, consistent to a standard asymptotic-preserving Fokker-Planck solver or an incompressible Navier-Stokes solver, only the conjugate–gradient method and fast Poission and Helmholtz solvers are needed. Numerical experiments are presented to demonstrate the accuracy and asymptotic behavior of the schemes, with several interesting applications.

Key words. Fluid–particles flows. Hydrodynamic regimes. Asymptotic Preserving Schemes. Kinetic-fluid model. Two-phase flow.

2010 MSC Subject Classification. 82C80 35Q35 82C40 76M20 65M06

1 Introduction

This paper is concerned with the simulation of a system of PDEs describing the evolution of disperse two-phase flows. While these flows can be modeled by a continuum description for all phases [30] we adopt here a kinetic–fluid modeling [40]. Such models are applicable to suspensions of solids as well as droplets. We use a kinetic description for the particulate phase and a hydrodynamic one for the underlying continuous fluid phase. Typical applications cover the dynamics of sprays [1, 2, 18, 39], particulate flows in fluidized beds [5], the calibration of fire prevention devices [44], environmental studies on pollutant transport [46, 48, 17, 42, 41, 45], combustion theory [40, 36, 49] and engine design [22, 35].

There exists a large variety of kinetic–fluid models, depending on the considered physical regime. Here and below, we adopt the following assumptions:

- The fluid phase is incompressible and viscous. For the sake of simplicity, we suppose that the fluid density is constant and homogeneous (see Remark 2.1 below).
- Both the fluid and particle phases are isothermal.
- We consider a single species of particles, with a given and fixed mass density and size.

[*]Project-Team SIMPAF, INRIA Lille Nord Europe Research Centre
[†]Labo P. Painlevé UMR 8524 CNRS & Université des Sciences et Technologies Lille 1 (thierry.goudon@inria.fr)
[‡]Department of Mathematics, University of Wisconsin Madison, WI 53706 (jin@math.wisc.edu, yan@math.wisc.edu)
[§]Department of Physics and Department of Mathematics, Duke University, Durham, NC 27708 (jliu@math.duke.edu)

- We assume there is no mass exchange between the phases, or in other words, the volume fraction occupied by the particles does not influence significantly the fluid density. According to [40], it corresponds to the so–called Thin Sprays modeling.
- Particles are subject to Brownian motion: according to [21, 20] it leads to diffusion with respect to the velocity variable in the equation for the particle distribution function.
- Each phase exerts an influence on the other phase through drag forces. Models for the drag forces are developed through experimental investigation and can have quite intricate expressions. Here we shall use the simplest Stokes formula where the drag force is proportional to the relative velocity $(v-u)$. An interesting derivation through homogenization arguments is discussed in [19].

Then, the flows are described by the fluid velocity field $u(t,x) \in \mathbb{R}^N$, depending on time $t \geq 0$ and space $x \in \mathbb{R}^N$, and the particle distribution function $f(t,x,v)$, which additionally depends on the (particle) velocity variable $v \in \mathbb{R}^N$. The evolution of the density f is governed by

$$\partial_t f + v \cdot \nabla_x f = \frac{1}{\varepsilon} L_u f + \nabla_x \Phi \cdot \nabla_v f, \tag{1}$$

where we have set

$$L_u f = \nabla_v \cdot \big((v-u) f + \nabla_v f \big). \tag{2}$$

A derivation of such an operator for particles in inhomogeneous flows is discussed in [24]. The evolution of the fluid obeys the Incompressible Navier-Stokes system

$$\begin{cases} \partial_t u + \nabla_x \cdot (u \otimes u) + \nabla_x p - \Delta_x u = \dfrac{1}{\varepsilon} \kappa \displaystyle\int (v-u) f \, \mathrm{d}v, \\ \nabla_x \cdot u = 0, \end{cases} \tag{3}$$

with $\kappa > 0$ a coupling constant that depends on the physical properties of the two phases.

The two phases are subject to external forces, embodied into the potential Φ. Of course, in the momentum equation (3), the external force term is incorporated within the pressure. Note however that the strength and the orientation of the external force might be different for the two phases. A relevant example is given by gravity driven flows where $\nabla_x \Phi$ is proportional to g, the gravitational acceleration. For the particles, the coefficient is $\eta_P = (1 - \rho_F/\rho_P)$ which accounts for the buoyancy force, with ρ_F and ρ_P (typical) densities of the fluid and the particles, respectively. The system (1)–(3) is written here in dimensionless form. The scaling parameter ε is associated to the Stokes settling time

$$\frac{2\rho_P a^2}{9\mu}$$

with μ the dynamic viscosity of the fluid, a the typical radius of the particles. We refer e.g. to [9, 11] for further details on the scaling issues.

The goal of the present paper is the design of a performing numerical scheme, able to handle different regimes, from $\varepsilon = O(1)$ (the kinetic regime) to $\varepsilon \ll 1$ (the hydrodynamic regime). As will be detailed below, in the hydrodynamic regime, the particle distribution function relaxes to the Maxwellian $\frac{n(t,x)}{(2\pi)^{N/2}} e^{-|v-u(t,x)|^2/2}$ and the limiting system for particle density n and particle macroscopic velocity u, which coincides to the fluid velocity, looks like the non homogeneous incompressible Navier–Stokes system, see (10)–(11).

Existence of weak solutions of system (1)–(3) has been investigated in [29] by fixed point methods and the theory has been revisited in [7] by using compactness techniques. Definitely, a difficulty relies on the construction of approximate solutions that preserve the conservation/dissipation properties of the model. We also refer to [37] for the analysis of compressible models. Smooth solutions close to equilibrium are studied in [28], see also [13] for a similar analysis of macroscopic models. The analysis of the asymptotics $\varepsilon \to 0$ in (1)–(3) is due to [26] by means of relative entropy methods,

see also [38]. It is also worth mentioning related works like the local existence of smooth solutions for the case without velocity–diffusion [3], several studies of coupling with the Euler system (i.e. viscosity is sensible only at the scale of the particles) [11, 12, 10] and systems with energy exchanges [6, 8, 27].

This work is organized as follows. In Section 2 we detail a few basic facts about the system (1)–(3) and the regime $\varepsilon \to 0$. In Section 3 we detail the construction of the numerical scheme. Our method takes place among the so–called "Asymptotic Preserving Schemes", a terminology coined in [31]. It means that the scheme is suitable for the kinetic equation in such a way that letting ε go to 0 while holding the mesh size and time step fixed, the scheme becomes a suitable scheme for the limiting equations. In particular, the stability constraints do not degenerate in the asymptotic regime. We refer to [32] for a recent review on the AP schemes and their applications. Roughly speaking the idea consists in evaluating implicitly the stiff terms of the equation. Here, it will require to invert the Fokker–Planck operator (2). To this end, we will follow the discretization introduced in [33]. Furthermore, our formulation of the scheme follows the framework of the projection method (see Chorin [14]–[16], Temam [47]), in the sense that only fast Helmholtz or Poisson solvers are needed, even with the implicit, nonlocal coupling terms between particles and the fluid. This is most natural when the incompressible fluid equations are solved by the projection method. The Fokker-Planck solver here, on the other hand, has a computational cost and complexity comparable to the previously developed AP scheme without the coupling to the fluid equation [33]. Both first and second order schemes are presented in this framework. Section 4 is devoted to the results of numerical simulations for checking accuracy, asymptotic behavior as well as some applications.

2 Hydrodynamic Limit

Let us briefly recall some basic facts about the system (1)–(3) and the regime $\varepsilon \to 0$. The key remark, observed in [25, 26], relies on the following energy–entropy dissipation property

$$\begin{aligned}\frac{\mathrm{d}}{\mathrm{d}t}\Big(\kappa \int_{\mathbb{R}^N\times\mathbb{R}^N} f\big(1+\Phi+v^2/2+\ln(f)\big)\,\mathrm{d}v\,\mathrm{d}x + \int_{\mathbb{R}^N} |u|^2/2\,\mathrm{d}x\Big)\\ + \int_{\mathbb{R}^N} |\nabla_x u|^2\,\mathrm{d}x + \frac{1}{\varepsilon}\int_{\mathbb{R}^N\times\mathbb{R}^N} \big|(v-u)\sqrt{f} + 2\nabla_v\sqrt{f}\big|^2\,\mathrm{d}v\,\mathrm{d}x \le 0.\end{aligned} \tag{4}$$

A similar relation holds when the problem is set on a bounded smooth domain Ω with reasonable boundary conditions. For instance we can assume no–slip of the fluid

$$u\Big|_{\partial\Omega} = 0 \tag{5}$$

and specular reflection of the particles

$$\gamma^- f(t,x,v) = \gamma^+ f\big(t,x,v-2v\cdot\hat\nu(x)\hat\nu(x)\big), \tag{6}$$

where $\hat\nu(x)$ stands for the unit outer normal at point $x\in\partial\Omega$ and $\gamma^\pm$ denote the trace operators on the set

$$\big\{(t,x,v)\in(0,\infty)\times\partial\Omega\times\mathbb{R}^N,\quad \pm v\cdot\hat\nu(x)>0\big\}.$$

We refer to further comments in [11]. It is worth rewriting the Fokker–Planck operator as

$$L_u f = \nabla_v\cdot\Big(M_u\nabla_v\Big(\frac{f}{M_u}\Big)\Big), \qquad M_u(v) = \frac{1}{(2\pi)^{N/2}}\exp\Big(-\frac{|v-u(t,x)|^2}{2}\Big).$$

As ε goes to 0, since the Fokker–Planck operator is penalized, we expect that f makes $L_u f$ (and the dissipation term in (4)) vanish which means that f becomes proportional to the Maxwellian centered to the fluid velocity

$$f(t,x,v)\simeq n(t,x)M_{u(t,x)}.$$

Hence the question is to identify the equation satisfied as $\varepsilon \to 0$ by the particles density n and the velocity u.

To this end, let us write the equations satisfied by the moments

$$n(t,x) = \int_{\mathbb{R}^N} f(t,x,v)\,\mathrm{d}v, \qquad J(t,x) = \int_{\mathbb{R}^N} v f(t,x,v)\,\mathrm{d}v.$$

Then one has

$$\partial_t n + \nabla_x \cdot J = 0, \tag{7}$$

$$\partial_t J + \nabla_x \mathbb{P} + n\nabla_x \Phi = -\frac{1}{\varepsilon}(J - nu) \tag{8}$$

where

$$\mathbb{P}(t,x) = \int_{\mathbb{R}^N} v \otimes v f(t,x,v)\,\mathrm{d}v.$$

Combined to (3) one obtains

$$\partial_t\Big(u + \kappa J\Big) + \nabla_x \cdot \Big(u \otimes u + \kappa \mathbb{P}\Big) + \nabla_x p + \kappa n \nabla_x \Phi = \Delta_x u. \tag{9}$$

Accordingly, when J and $\mathbb{P}$ are asymptotically defined by the moments of the Maxwellian nM_u, one is led to

$$J \simeq nu, \qquad \mathbb{P} \simeq nu \otimes u + n\mathbb{I}.$$

Inserting this ansatz into (9) one arrives at

$$\partial_t\Big(\Big(1 + \kappa n\Big)u\Big) + \nabla_x \cdot \Big(\Big(1 + \kappa n\Big)u \otimes u\Big) + \nabla_x\Big(p + \kappa n\Big) + \kappa n \nabla_x \Phi = \Delta_x u, \tag{10}$$

where the velocity is still required to be divergence free while for the density of particles

$$\partial_t n + \nabla_x \cdot (nu) = 0. \tag{11}$$

The system (10)–(11) is (up to the gravity term) nothing but the incompressible Navier-Stokes system for the composite and inhomogeneous density $(1 + \kappa n)$. Of course a rigorous justification of the convergence statement presents technical difficulties, due to the nonlinear passages to the limit it requires, in particular with the product $nu \otimes u$. We refer to [26] for a proof based on relative entropy arguments and to [37, 38, 11] where related questions are discussed.

Remark 2.1 *Note that the problem does not simplify if we start with the Stokes equation for the fluid instead of* (3)*, because the convection term in the limit equation comes anyway from the kinetic pressure* $\mathbb{P}$*. We point out also that it makes sense to consider from the beginning that the fluid density* $\rho(t,x)$ *is non homogeneous. In such a case* (3) *is replaced by*

$$\begin{aligned}
&\partial_t \rho + \nabla_x \cdot (\rho u) = 0,\\
&\partial_t(\rho u) + \nabla_x \cdot (\rho u \otimes u) + \nabla_x p + \eta_F \rho \nabla_x \tilde{\Phi} = \Delta_x u + \frac{1}{\varepsilon}\kappa \int_{\mathbb{R}^N} (v - u) f\,\mathrm{d}v,
\end{aligned}$$

coupled to the divergence free constraint $\nabla_x \cdot u = 0$*. Here* $\nabla_x \tilde{\Phi} = \frac{1}{\eta_P}\nabla_x \Phi = g$*. Note the coefficient* η_F*, potentially different from* η_P*, characterizes the effect of the external forces on the fluid. The limiting problem will be of the same type for the composite density* $\rho + \kappa n$*; namely one obtains as* $\varepsilon \to 0$

$$\begin{aligned}
&\partial_t \rho + \nabla_x \cdot (\rho u) = 0 = \partial_t n + \nabla_x \cdot (nu) = 0,\\
&\partial_t\Big(\Big(1 + \kappa n\Big)u\Big) + \nabla_x \cdot \Big(\Big(1 + \kappa n\Big)u \otimes u\Big) + \nabla_x\Big(p + \kappa n\Big) + (\eta_F \rho + \eta_P n)\nabla_x \tilde{\Phi} + \Delta_x u,\\
&\nabla_x \cdot u = 0.
\end{aligned}$$

3 An AP Scheme for the Flowing Regime

As announced in the Introduction, we wish to construct a numerical scheme for (1)–(3), with the specific request to capture the asymptotic regime $\varepsilon \to 0$ efficiently. In particular, as ε goes to 0, the scheme should become a robust solver for the limit system (10)–(11). Furthermore, the asymptotic regime should not introduce prohibitive numerical constraints, by having the stability condition independent of ε. A scheme that fulfills these requirements is said Asymptotic Preserving [31, 23, 32]. Roughly speaking, the idea is to evaluate implicitly the stiff terms in the equations, namely the drag force in (3) and the Fokker–Planck operator in (1). The key point of the method that provides the AP property to the scheme relies on a convenient time splitting which allows to compute implicitly the stiff terms efficiently. Recall that an AP scheme for the Fokker-Planck equation, developed in [33], relies just on a conjugate gradient method for the implicit Fokker-Planck operator, while a typical incompressible Navier-Stokes solver, such as the projection method, requires a fast Poisson or Helmholtz solver. For the problem under study, even if more implicit coupling terms are involved than the problems studied previously, our AP schemes do not require more than the conjugate gradient method and a fast Poisson or Helmholtz solver.

3.1 Projection method

The projection method for the incompressible Navier-Stokes system (3) contains two steps. First, the equation without pressure term is solved with a suitable boundary condition on u^*,

$$\frac{u^* - u^k}{\Delta t} + \nabla_x \cdot (u^k \otimes u^k) - \Delta_x u^* = S^{k,k+1}.$$

Then u^* is projected to the divergence free space,

$$\frac{u^{k+1} - u^*}{\Delta t} + \nabla_x p^{k+1} = 0$$

with $\nabla_x \cdot u^{k+1} = 0$. This step is solved by first computing p^{k+1}:

$$\Delta_x p^{k+1} = \frac{1}{\Delta t} \nabla_x \cdot u^*$$

with a suitable boundary condition (for example, the Neumann boundary condition $\frac{\partial p}{\partial \tilde{\nu}} = 0$). Then

$$u^{k+1} = u^* - \Delta t \nabla_x p^{k+1}.$$

This is a first order projection scheme in time ([14, 15, 16], [47]). Higher order schemes can be derived ([34], [4]).

In this Section $S^{k,k+1}$ is considered as a given data. For our purposes however, it will depend on the velocity field through the drag force terms, which will modify the structure of the linear problems that govern the updating of the velocity.

3.2 Construction of the AP Schemes

The AP scheme works in two steps. Firstly we update the macroscopic quantities n, J, u, p and secondly we update the microscopic density of particles. The former leads to invert a coupled linear system. The latter needs to invert the Fokker–Planck operator, which relies on a specific discretization to obtain a structure appropriate for using performing algorithms.

To start with, we compute the macroscopic density of particles,

$$\frac{1}{\Delta t}(n^{k+1} - n^k) = -\int v \cdot \nabla_x f^k \, \mathrm{d}v = -\nabla_x \cdot J^k. \tag{12}$$

Next we apply the projection method to the momentum equation (8) with the incompressible Navier-Stokes equation (3). We solve

$$\frac{1}{\Delta t}(J^* - J^k) = -\int v \otimes v \nabla_x f^k \,\mathrm{d}v - n^k \nabla_x \Phi - \frac{1}{\varepsilon}\big(J^* - n^{k+1}u^*\big), \tag{13a}$$

$$\frac{1}{\Delta t}(u^* - u^k) - \Delta_x u^* = -\nabla_x \cdot (u^k \otimes u^k) + \frac{1}{\varepsilon}\kappa\big(J^* - n^{k+1}u^*\big). \tag{13b}$$

This is equivalent to solve

$$\left(\frac{1}{\Delta t} + \frac{1}{\varepsilon + \Delta t}\kappa n^{k+1} - \Delta_x\right) u^* = \frac{u^k}{\Delta t} - \nabla_x \cdot (u^k \otimes u^k) + \frac{1}{\varepsilon + \Delta t}\kappa\big(J^k - \Delta t \int v \otimes v \nabla_x f^k \,\mathrm{d}v\big). \tag{14}$$

The no–slip boundary condition for u^* is used,

$$u^*\Big|_{\partial\Omega} = 0. \tag{15}$$

(14) is a variable coefficient Helmholtz equation for u^*, which can be solved by the Preconditioned Conjugate Gradient method without difficulties (for example, see [43]). Then u^* is projected to the divergence free space,

$$\Delta_x p^{k+1} = \frac{1}{\Delta t}\nabla_x \cdot u^*, \quad \frac{\partial p^{k+1}}{\partial \hat{\nu}}\Big|_{\partial\Omega} = 0, \tag{16}$$

$$u^{k+1} = u^* - \Delta t \nabla_x p^{k+1}. \tag{17}$$

Equation (16) is solved by the FFT method. From (17), $u^{k+1} = O(\Delta t)$ at boundary. The first order accuracy is preserved. Finally f^{k+1} is solved based on the kinetic equation (1), with a fully implicit Fokker-Panck operator

$$\frac{f^{k+1} - f^k}{\Delta t} + v \cdot \nabla_x f^k - \nabla_x \Phi \cdot \nabla_v f^k = \frac{1}{\varepsilon} L_{u^{k+1}} f^{k+1}, \tag{18}$$

where

$$L_{u^{k+1}} f^{k+1} = \nabla_v \cdot ((v - u^{k+1}) f^{k+1} + \nabla_v f^{k+1}).$$

Then J^{k+1} is updated by taking the first moment of f^{k+1}.

This is a *predictor-corrector* method for the kinetic equation (1). One first predicts the momentum at t^{k+1} by solving for u^*. Then the divergence free velocity u^{k+1} is derived and the momentum J^{k+1} at t^{k+1} is corrected accordingly. The only constraint on time step is the CFL condition from the transport part of kinetic equation (1), i.e. $\Delta t \le \frac{\Delta}{\max |v|}$, with Δ the space mesh size.

3.3 A second order scheme

Equations (12)–(18) give a first order scheme. We can generalize it to second order. The convergence order can be improved by the following techniques.

- The time derivative terms are approximated by a second order BDF method, i.e.,

$$\partial_t a(t^{k+1}) \approx \frac{3a^{k+1} - 4a^k + a^{k-1}}{2\Delta t};$$

- The transport terms are approximated by extrapolation from last two steps, i.e.,

$$b(t^{k+1}) \approx 2b^k - b^{k-1};$$

- The stiff terms are implicitly formulated at t^{k+1};

- u^* is solved with the boundary condition $u^* \cdot \hat{\nu} = 0$, $u^* \cdot \hat{\tau} = \Delta t \dfrac{\partial p^k}{\partial \hat{\tau}}$, where $\hat{\tau}(x)$ is the unit tangent vector at point $x \in \partial\Omega$. This ensures that the projection step only introduces second order error (see [34]).

We describe the detailed scheme now. First, the macroscopic density of particles is computed by,

$$\frac{1}{2\Delta t}(3n^{k+1} - 4n^k + n^{k-1}) = -\int v \cdot \nabla_x (2f^k - f^{k-1})\,\mathrm{d}v = -\nabla_x \cdot (2J^k - J^{k-1}). \tag{19}$$

Next we solve the coupled momentum equations (8) with (3), without pressure term,

$$\begin{aligned}
&\frac{1}{2\Delta t}(3J^* - 4J^k + J^{k-1}) = -\int v \otimes v \nabla_x (2f^k - f^{k-1})\,\mathrm{d}v - (2n^k - n^{k-1})\nabla_x \Phi - \frac{1}{\varepsilon}\big(J^* - n^{k+1}u^*\big),\\
&\frac{1}{2\Delta t}(3u^* - 4u^k + u^{k-1}) - \Delta_x u^* = -\nabla_x \cdot (2u^k \otimes u^k - u^{k-1} \otimes u^{k-1}) + \frac{1}{\varepsilon}\kappa\big(J^* - n^{k+1}u^*\big).
\end{aligned}$$

This is equivalent to solve

$$\begin{aligned}
\left(\frac{3}{2\Delta t} + \frac{3}{3\varepsilon + 2\Delta t}\kappa n^{k+1} - \Delta_x\right) u^* = {} & \frac{4u^k - u^{k-1}}{2\Delta t} - \nabla_x \cdot (2u^k \otimes u^k - u^{k-1} \otimes u^{k-1}) \\
& + \frac{1}{3\varepsilon + 2\Delta t}\kappa \left\{ 4J^k - J^{k-1} - 2\Delta t \left(\int v \otimes v \nabla_x (2f^k - f^{k-1})\,\mathrm{d}v + (2n^k - n^{k-1})\nabla_x \Phi \right) \right\}.
\end{aligned} \tag{20}$$

The following boundary condition for u^* is used on $\partial\Omega$,

$$u^* \cdot \hat{\nu} = 0, \qquad u^* \cdot \hat{\tau} = \Delta t \frac{\partial p^k}{\partial \hat{\tau}}. \tag{21}$$

Equation (20) can be solved by the Preconditioned Conjugate Gradient method without difficulties. Then u^* is projected to the divergence free space,

$$\Delta_x p^{k+1} = \frac{1}{\Delta t}\nabla_x \cdot u^*, \quad \frac{\partial p^{k+1}}{\partial \hat{\nu}} = 0, \tag{22}$$

$$u^{k+1} = u^* - \Delta t \nabla_x p^{k+1}, \tag{23}$$

where p^{k+1} is solved by the FFT method. Notice that u^{k+1} satisfies

$$\begin{aligned}
u^{k+1} \cdot \hat{\nu} &= u^* \cdot \hat{\nu} - \Delta t \frac{\partial p^{k+1}}{\partial \hat{\nu}} = 0,\\
u^{k+1} \cdot \hat{\tau} &= u^* \cdot \hat{\tau} - \Delta t \frac{\partial p^{k+1}}{\partial \hat{\nu}} = \Delta t \frac{\partial}{\partial \hat{\nu}}(p^k - p^{k+1}) = O(\Delta t^2),
\end{aligned}$$

thus a second order accuracy on boundary is achieved.

Finally f^{k+1} is solved based on the kinetic equation (1),

$$\frac{3f^{k+1} - 4f^k + f^{k-1}}{2\Delta t} + (v \cdot \nabla_x - \nabla_x \Phi \cdot \nabla_v)(2f^k - f^{k-1}) = \frac{1}{\varepsilon} L_{u^{k+1}} f^{k+1}, \tag{24}$$

and J^{k+1} is updated by taking the first moment of f^{k+1}.

Equations (19)–(24) give a second order scheme in time. We will check this convergence order numerically in Section 4.1.

Remark 3.1 *Note that this second order scheme is a Multistep method. To compute the solutions at t^{k+1}, we need the solutions from both t^k and t^{k-1}. Therefore, with initial data at t^0, it is necessary to apply the first order method to obtain the solutions at t^1. Then this second order scheme can be started.*

3.4 The AP property

Now we show that the first order scheme (12)–(18) is asymptotic preserving and the limiting scheme gives a first order approximation for the limiting system (10)–(11).

As $\varepsilon \to 0$, (18) gives

$$L_{u^{k+1}} f^{k+1} = O(\varepsilon), \quad \text{for } k \geq 0.$$

This is equivalent to

$$f^k = n^k M_{u^k} + O(\varepsilon), \quad \text{for } k \geq 1.$$

Then one has

$$J^k = n^k u^k + O(\varepsilon),$$

$$\int_{\mathbb{R}^N} v \otimes v f^k \, \mathrm{d}v = n^k u^k \otimes u^k + n^k \mathbb{I} + O(\varepsilon).$$

Therefore, (12) is just

$$\frac{1}{\Delta t}(n^{k+1} - n^k) = -\nabla_x \cdot (n^k u^k) + O(\varepsilon). \tag{25}$$

Besides, equation (13a) gives

$$J^* = n^{k+1} u^* + O(\varepsilon).$$

Multiply (13a) by κ and add to (13b). One obtains,

$$\begin{aligned} \frac{1}{\Delta t}\left(\left(1+\kappa n^{k+1}\right) u^* - \left(1+\kappa n^k\right) u^k\right) - \Delta_x u^* = \\ -\nabla_x \cdot \left(\left(1+\kappa n^k\right) u^k \otimes u^k\right) - \kappa \nabla_x n^k - \kappa n^k \nabla_x \Phi + O(\varepsilon). \end{aligned} \tag{26}$$

Equation (25) and (26) give a first order discretization of the limiting system (10)–(11). The divergence free condition on u^k is guaranteed by (16) and (17).

Similarly, one can show the limiting of the second order scheme (19)–(24) gives a second order approximation for the limiting system (10)–(11). We omit the details.

3.5 Full discretization

3.5.1 Space and velocity discretization

For the sake of concreteness, let us discuss space and velocity discretization issues by restricting to the two–dimension case. The extension to higher dimension is straightforward. We denote by Δx the (uniform) mesh size. We define a regularly spaced and symmetric velocity grid, with step Δv. Denoting $\mathbf{j} = (j, j')$ and $\mathbf{m} = (m, m')$ in $\mathbb{N}^2$, $f^k_{\mathbf{j};\mathbf{m}}$ stands for the numerical approximation of $f(k\Delta t, \mathbf{j}\Delta x, \mathbf{m}\Delta v)$.

For the transport term $v \cdot \nabla_x f$ in (18) and (24), we apply the upwind type second order shock capturing schemes (see [27]). Discrete differential operators are defined dimension-by-dimension.

The specular reflection law is used to define the ghost points. For instance, labeling the numerical unknown with indices $j, j' \in \{1, ..., J\}$ and $m \in \{1, ..., 2M+1\}$, where the M first (resp. last) velocities are negative (resp. positive), leads to

$$f^k_{0,j';m,m'} = f^k_{1,j';2M+2-m;m'}, \qquad f^k_{J+1,j';m,m'} = f^k_{J,j';2M+2-m,m'}$$

and similar expression when exchanging the role of j, j' and m', m'.

The convection term $\nabla_x \cdot (u \otimes u)$ and the diffusion term $\Delta_x u$ in incompressible Navier-Stokes system (3), as well as the terms $\nabla_x \cdot u^*$ and $\nabla_x p$ in the projection steps (16)–(17) and (22)–(23), are approximated by center differences.

Macroscopic quantities are defined by using the 2–dimensional version of the trapezoidal rule in order to ensure that the even moments of the odd functions with respect to v vanish.

The derivative with respect to velocity which appears in the acceleration term is also solved by the upwind type second order shock capturing schemes (see [27]).

3.5.2 Inversion of the Fokker-Planck operator

We have already discussed the discretization of the transport term. Now we focus on how to solve f^{k+1} from (18), where the stiff term is treated implicitly. We need to invert the Fokker–Planck operator. To this end, we follow the approach introduced in [33]. We write

$$L_u f = \sqrt{M_u}\ \tilde{L}_u h$$

with

$$h = \frac{f}{\sqrt{M_u}}, \qquad \tilde{L}_u h = \frac{1}{\sqrt{M_u}} \nabla_v \cdot \Big(M_u \nabla_v \Big(\frac{h}{\sqrt{M_u}} \Big) \Big).$$

Note that $\tilde{L}_u$ is symmetric for the standard L^2 inner product

$$\int_{\mathbb{R}^N} \tilde{L}_u h\ g \,\mathrm{d}v = \int_{\mathbb{R}^N} h\ \tilde{L}_u g \,\mathrm{d}v.$$

Accordingly, we set

$$h_{\mathbf{j};\mathbf{m}} = \frac{f^{k+1}_{\mathbf{j};\mathbf{m}}}{\sqrt{M^{k+1}_{\mathbf{j};\mathbf{m}}}}, \qquad \mathscr{L} f^{k+1}_{\mathbf{j};\mathbf{m}} = \sqrt{M^{k+1}_{\mathbf{j};\mathbf{m}}}\ \tilde{\mathscr{L}} h_{\mathbf{j};\mathbf{m}}.$$

The discrete operator $\tilde{\mathscr{L}}$ is symmetric which allows to make use of the Conjugate Gradient algorithm. In dimension two, the discrete operator $\tilde{\mathscr{L}}$ is defined as follows

$$\begin{aligned}
\tilde{\mathscr{L}} h_{j,j';m,m'} &= \frac{1}{\Delta v^2} \left(h_{j,j';m,m'+1} + h_{j,j';m+1,m} - \overline{M}^{k+1}_{j,j';m,m'} h_{j,j';m,m'} + h_{j,j';m,m'-1} + h_{j,j';m-1,m'} \right), \\
\overline{M}^{k+1}_{j,j';m,m'} &= \frac{\sqrt{M^{k+1}_{j,j';m+1,m'}} + \sqrt{M^{k+1}_{j,j';m,m'+1}} + \sqrt{M^{k+1}_{j,j';m-1,m'}} + \sqrt{M^{k+1}_{j,j';m,m'-1}}}{\sqrt{M^{k+1}_{j,j';m,m'}}}
\end{aligned} \tag{27}$$

which indeed leads to a symmetric matrix. Observe that $\tilde{\mathscr{L}}\big(\sqrt{M^{k+1}}\big)_{\mathbf{j};\mathbf{m}} = 0$. Therefore, the updating of the particles distribution function

$$\big(1 - \frac{\Delta t}{\varepsilon} \mathscr{L}\big) f^{k+1}_{\mathbf{j};\mathbf{m}} = S^k_{\mathbf{j};\mathbf{m}}$$

obeys the following rules:

- Solve the linear system
$$\big(1 - \frac{\Delta t}{\varepsilon} \tilde{\mathscr{L}}\big) h_{\mathbf{j};\mathbf{m}} = \frac{S^k_{\mathbf{j};\mathbf{m}}}{\sqrt{M^{k+1}_{\mathbf{j};\mathbf{m}}}}.$$
- Set $f^{k+1}_{\mathbf{j};\mathbf{m}} = h_{\mathbf{j};\mathbf{m}} \sqrt{M^{k+1}_{\mathbf{j};\mathbf{m}}}$.

4 Numerical simulations

From now on we will use the following notations: $\mathbf{x} = (x, y)$ is the position variable, $\mathbf{v} = (v_1, v_2)$ is the velocity variable, $\mathbf{u} = (u_1, u_2)$ is the fluid velocity and $\mathbf{u}_p = (u_{p1}, u_{p2})$ is the macroscopic particle velocity.

We apply the second order method described in Section 3.3. Unless otherwise specified, we always use the following settings.

The computation is performed on $(\mathbf{x}, \mathbf{v}) \in [0, 1]^2 \times [-v_{\max}, v_{\max}]^2$, with $v_{\max} = 6$. The specular boundary condition is applied on particle distribution f, while no-flip boundary condition is used for fluid velocity $\mathbf{u}$.

We take $N_x = 30$ grid points in each x direction and $N_v = 32$ grid points in each v direction. We apply the van Leer type slope limiter on the discretization of the advection parts, and take $\Delta t = \frac{\Delta x}{5v_{\max}}$, which guarantees the stability.

We always take

$$f(0, \mathbf{x}, \mathbf{v}) = n(0, \mathbf{x}) M_{\mathbf{u}_p(0,\mathbf{x})}$$

as the initial data for particles distribution. Here $\mathbf{u}_p = \frac{J}{n}$ is the macroscopic velocity of particles. Note that this is not necessary the equilibrium in the sense that $L_{\mathbf{u}} f \neq 0$ in (2) since we do not require $\mathbf{u}_p = \mathbf{u}$.

We take $\kappa = 2$ throughout the simulations. However the schemes can be applied to the case when κ is very large, without any difficulty.

4.1 Convergence Order

First we numerically check that the scheme described in Section 3.3 is indeed second order in Δx (therefore in Δt). We start with the initial data

$$\begin{aligned} &n(0, \mathbf{x}) = 0.5 + \exp\left(-20(x-0.5)^2 - 20(y-0.5)^2\right), \\ &\mathbf{u}_p(0, \mathbf{x}) = \begin{pmatrix} -\sin(2\pi(y-0.5)) \\ \sin(2\pi(x-0.5)) \end{pmatrix} \exp\left(-20(x-0.5)^2 - 20(y-0.5)^2\right), \\ &\mathbf{u}(0, \mathbf{x}) = 0. \end{aligned} \tag{28}$$

We compute the solutions on a grid of $N_x \times N_x \times N_v \times N_v$, with $N_x = 16, 32, 64, 128$ respectively. As mentioned before, $N_v = 32$. After time $t_{\max} = 0.033$ we check the following error,

$$\begin{aligned} e_{\Delta x}(f) &= \max_{t \in (0, t_{\max})} \frac{||f_{\Delta x}(t) - f_{2\Delta x}(t)||_p}{||f_{2\Delta x}(0)||_p}, \\ e_{\Delta x}(\mathbf{u}) &= \max_{t \in (0, t_{\max})} \frac{||\mathbf{u}_{\Delta x}(t) - \mathbf{u}_{2\Delta x}(t)||_p}{||\mathbf{u}_{2\Delta x}(t_{\max})||_p}. \end{aligned} \tag{29}$$

This can be considered as an estimation of the relative error in L^p norm, where $f_{\Delta x}$ and $\mathbf{u}_{\Delta x}$ are the numerical solutions computed from a grid of size $\Delta x = \frac{1}{N_x}$. The numerical scheme is said to be k-th order if $e_{\Delta x} \leq C \Delta x^k$, for Δx small enough.

Figure 1 gives the convergence order in L^1 norm, showing that the scheme is almost second order in space (hence in time) **uniformly in** ε, as expected. The convergence order is 1.7 for particle distribution function f and 1.6 for the fluid velocity $\mathbf{u}$.

4.2 AP Property

Now we check the AP property we proposed in Section 3.4. We take the volcano like initial data

$$\begin{aligned} &n(0, \mathbf{x}) = (0.5 + 100((x-0.5)^2 + (y-0.5)^2)) \exp\left(-40(x-0.5)^2 - 40(y-0.5)^2\right), \\ &\mathbf{u}_p(0, \mathbf{x}) = \begin{pmatrix} -\sin(2\pi(y-0.5)) \\ \sin(2\pi(x-0.5)) \end{pmatrix} \exp\left(-20(x-0.5)^2 - 20(y-0.5)^2\right), \\ &\mathbf{u}(0, \mathbf{x}) = 0. \end{aligned} \tag{30}$$

Therefore initially $\mathbf{u}_p \neq \mathbf{u}$ and the equilibrium is not assumed. We apply the second order scheme and perform the simulation until $t = 0.5$. In Figure 2, where $\varepsilon = 1$, we show the pictures of particle density n, streamlines of particle velocity $\mathbf{u}_p$ and fluid velocity $\mathbf{u}$ at t^0 (the initial time), t^1 (after one time step) and t^{450} (the end time). The streamlines of particles and fluid are totally different. The particles expand to the whole square domain and are not significantly affected by the circulating fluid. We show the same quantities in Figure 3 with $\varepsilon = 10^{-5}$. In this case the drag force between different phases is so strong that the particles also circulate in the square domain.

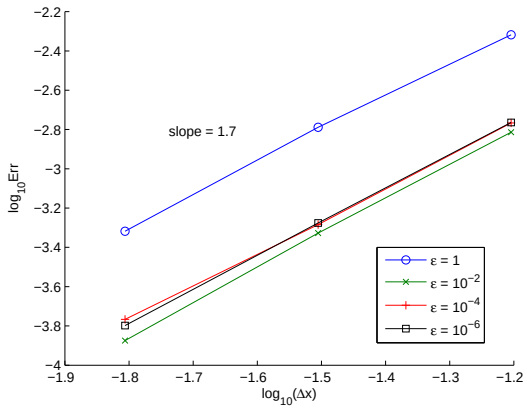

(a) Convergence of particle distribution f.

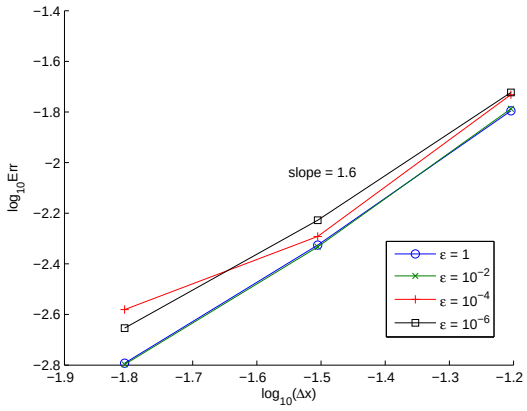

(b) Convergence of fluid velocity $\mathbf{u}$.

Figure 1: The test of convergence order with initial data (28). This figure shows the l^1 errors (29) in particle distribution f (left) and fluid velocity $\mathbf{u}$ (right) with different ε.

Besides, the expansion in particle density is decelerated by the fluid. The particles keep the volcano shape well in this period of time.

At last, we check the time evolution of L^1 distances $||f - nM_{\mathbf{u}}||_1$. Note that $M_{\mathbf{u}}$ is a Maxwellian centered at the fluid velocity $\mathbf{u}$. The result is shown in Figure 4. As expected, we have $f - nM_{\mathbf{u}} = O(\varepsilon)$ after one time step. This gives a direct evidence of the AP property we proposed.

4.3 Some Applications

Our schemes are easily extended to more complicated circumstances. In this section we apply our schemes to several different problems. In section 4.3.1 the external force (the gravity) is considered. In section 4.3.2 a different boundary condition is applied on particle distribution f, while in section 4.3.3 we apply a different boundary condition on fluid velocity $\mathbf{u}$.

4.3.1 Simulation with a dam like initial data

Now we consider the dam like initial data,

$$\begin{aligned} &n(0,\mathbf{x}) = 10^{-10} + \mathbf{1}_{0\le x\le 0.5},\\ &\mathbf{u}_p(0,\mathbf{x}) = 0,\\ &\mathbf{u}(0,\mathbf{x}) = 0. \end{aligned}$$

In this case the movement of particles and fluid are initiated by the gravity. We include the external force term $\nabla_x\Phi\cdot\nabla_v f$ in our simulation, where $\Phi = gy$ with gravity constant $g = 10$. The particles are uniformly distributed in the left hand side. As the simulation starts, the particles fall down and cause the circulation of fluid.

Figure 5(a) shows the time evolution of particle density when $\varepsilon = 1$. Figure 5(b) shows the streamlines of velocity of particles and fluid at the end of simulation. In this case the drag force between particles and fluid is not significant. The particles just fall down and concentrate in the left part of bottom. Figure 5(b) shows clearly the behavior of particles is quite different from that of the fluid.

Figure 6(a) shows the time evolution of particle density when ε is quite small, $\varepsilon = 10^{-5}$. Figure 6(b) shows the streamlines of velocity of particles and fluid at the end of simulation. In this case the drag force between particles and fluid is so strong that the particles and the fluid keep the same

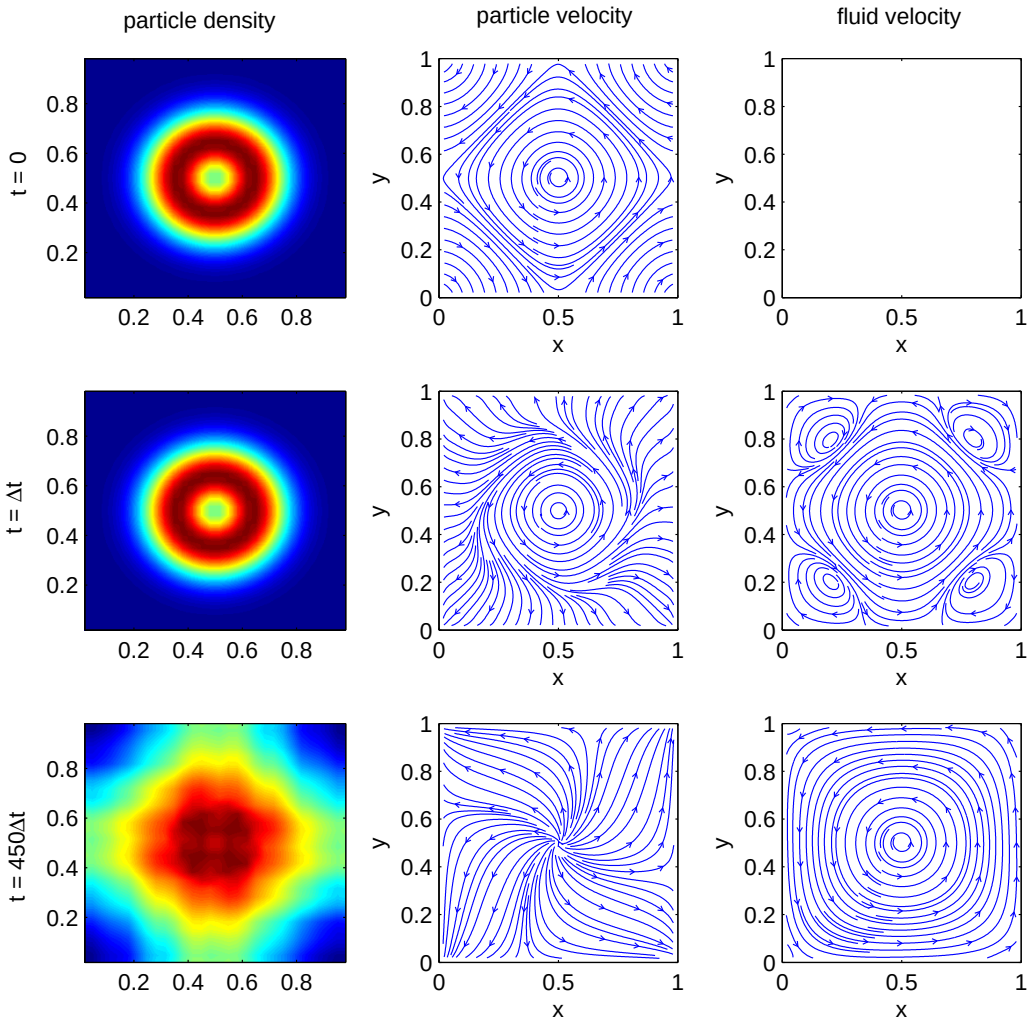

Figure 2: The test of AP property with initial data (30) for $\varepsilon = 1$. This figure shows the particle density n (left column), streamlines of particle velocity $\mathbf{u}_p$ (middle column) and fluid velocity $\mathbf{u}$ (right column) at $t = 0$ (upper row), $t = \Delta t$ (middle row) and $t = 450\Delta t$ (lower row). The gravity is neglected.

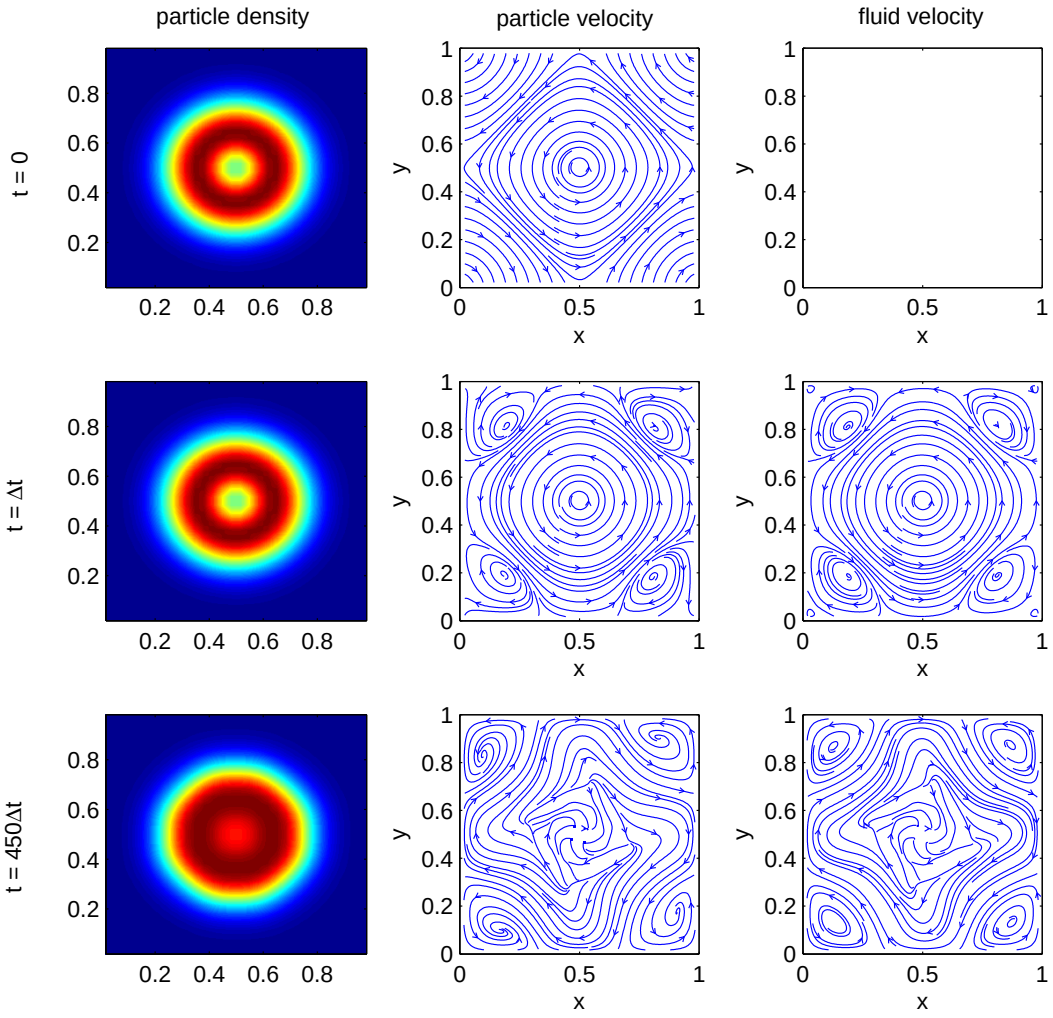

Figure 3: The test of AP property with initial data (30) for $\varepsilon = 10^{-5}$. This figure shows the particle density n (left column), streamlines of particle velocity $\mathbf{u}_p$ (middle column) and fluid velocity $\mathbf{u}$ (right column) at $t = 0$ (upper row), $t = \Delta t$ (middle row) and $t = 450\Delta t$ (lower row). The gravity is neglected.

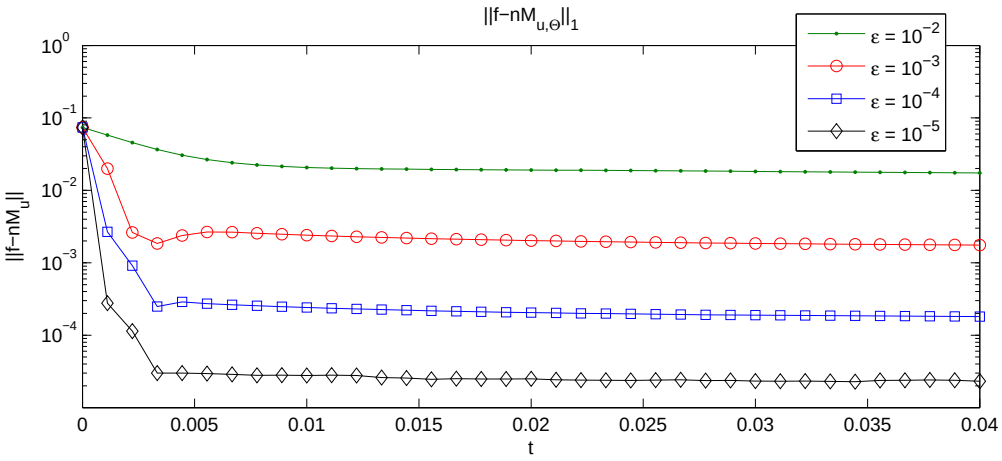

Figure 4: The time evolution of $||f - nM_{\mathbf{u}}||_1$ with different ε, starting with the initial data (30).

pace. As time evolves, the particles fall down and drive the fluid to circulate counter-clockwisely. Then the particles follow this circulation and show an S-shape curve. Finally the particles settle at the bottom uniformly due to the loss of energy.

4.3.2 Simulation of Injecting Problem

Now let us consider the situation when the particles are injected into the square domain. We take the initial data as follows.

$$n(0, \mathbf{x}) = 10^{-10}, \quad \mathbf{u}_p(0, \mathbf{x}) = \mathbf{u}(0, \mathbf{x}) = 0.$$

The injecting particle flow is described by the boundary condition on f,

$$f(t, \mathbf{x}, \mathbf{v}) = 1_{2 \le v_1 \le 3}, \quad \text{if } \mathbf{x} \in \Gamma$$

where v_1 is the first component of $\mathbf{v}$. The entrance of flow Γ locates at the center of the left boundary,

$$\Gamma = \{(0, y) | 0.45 \le y \le 0.55\}.$$

We perform the simulation with different ε. In Figure 7 we show the particle density (left) and streamlines of particle velocity (middle) and fluid velocity (right) at time $t = 0.5$. We ignore the gravity effect.

In Figure 7(a), where $\varepsilon = 1$, the particles spread to the right end of the domain. The streamlines of fluid and particles are totally different, which suggests the interaction between them are not obvious. Besides, the streamline of particle velocity at the right end seems to show that the particles are flowing out of the domain. However we would like to point out that the particle velocity is very close to 0 at this end. One may observe that the particles are actually accumulating at the right end of the domain, from the left picture of Figure 7(a).

In Figure 7(b), where $\varepsilon = 10^{-2}$, the spreading of particles to the right end is decelerated by the strong drag force from the fluid. From the streamline of particle velocity (the middle figure), the whole domain is divided into two parts. The left half of the domain contains incoming particles and the streamline behaves similarly as in the case $\varepsilon = 1$ (see the middle picture in Figure 7 (a)). The right half of the domain only contains the particles which are initially uniformly placed in the whole domain ($n = 10^{-10}$). The streamline behaves similarly to that of the fluid (see the right half of the right picture in Figure 7 (b)). As time evolves, the left half would gradually expand to the whole domain.

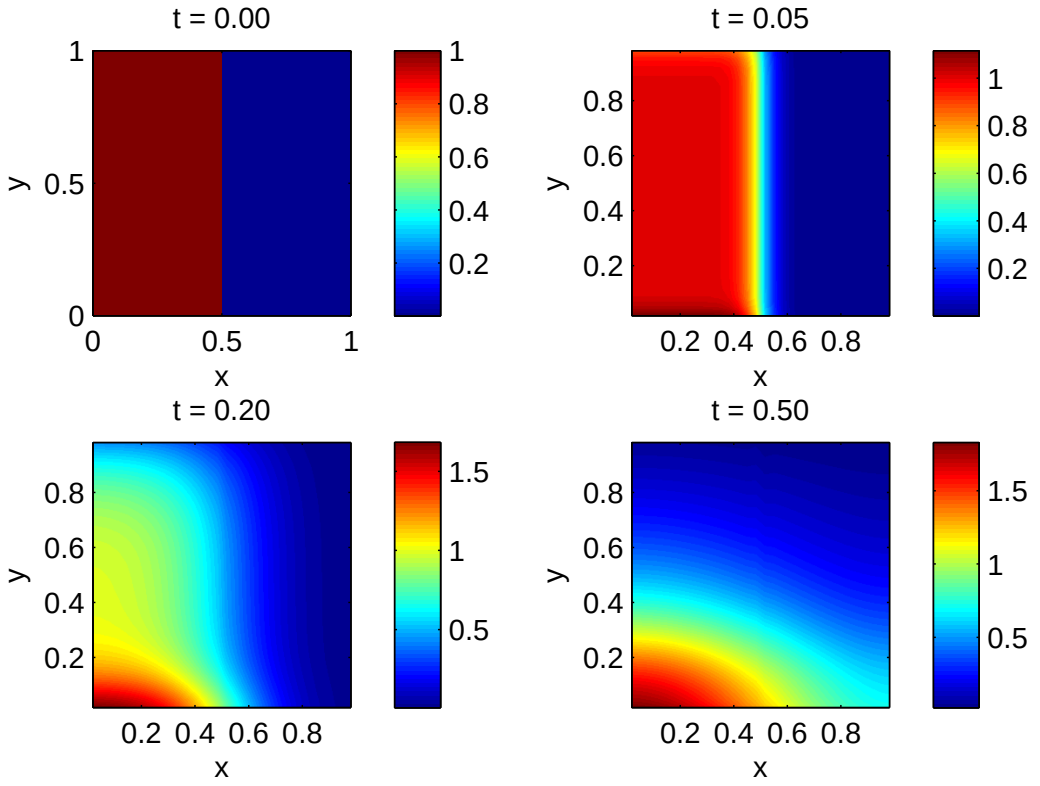

(a) Particle density.

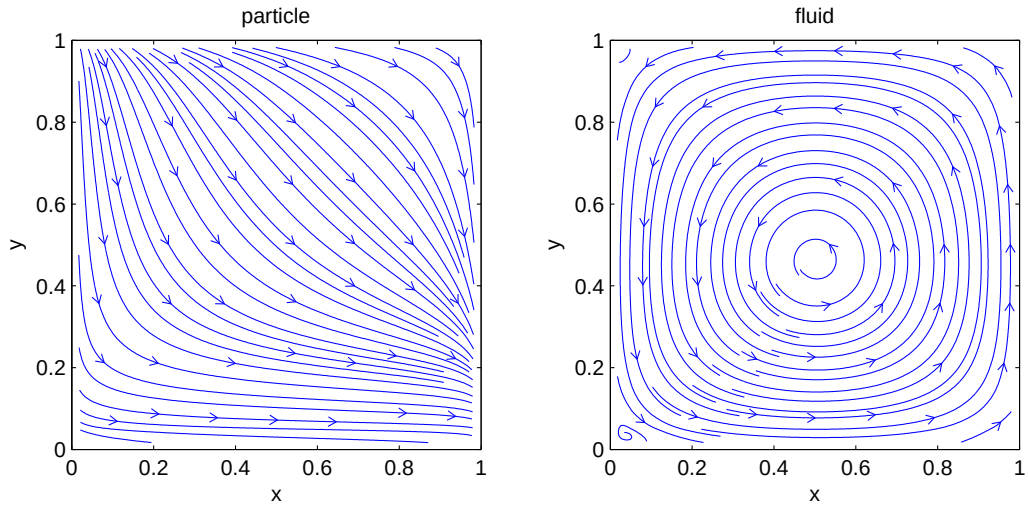

(b) Streamlines.

Figure 5: Part (a) shows the time evolution of particle density corresponding to the dam like initial data. Part (b) shows the streamlines of velocities of particles (left) and fluid (right) after time $t = 0.5$. $\varepsilon = 1$. The gravity is considered.

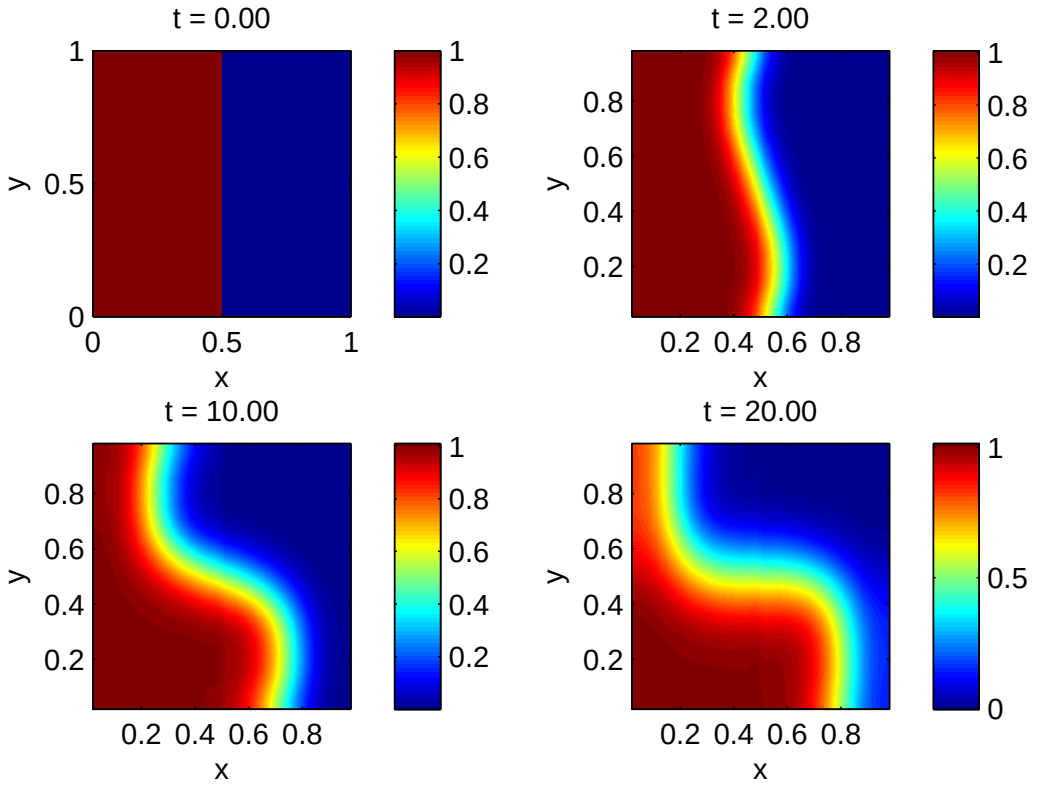

(a) Particle density.

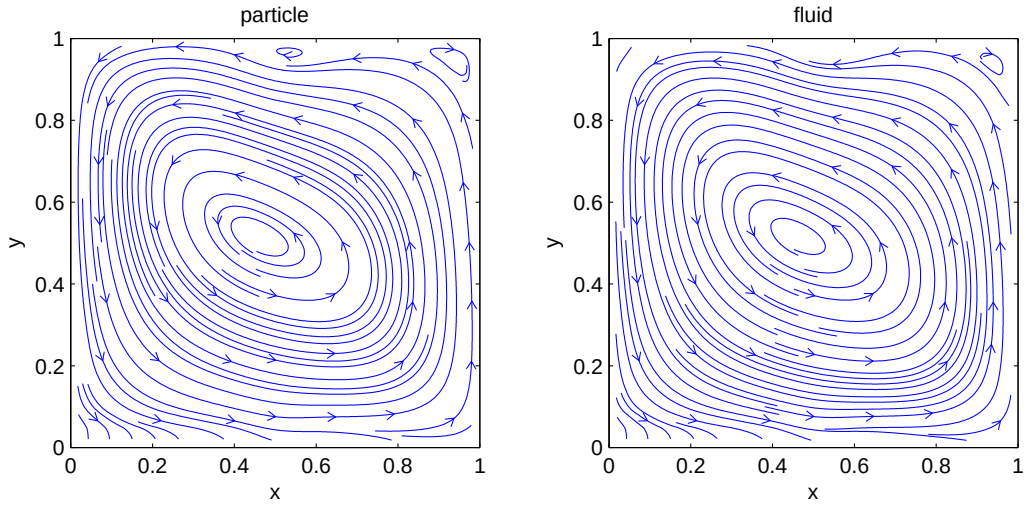

(b) Streamlines.

Figure 6: Part (a) shows the time evolution of particle density corresponding to the dam like initial data. Part (b) shows the streamlines of velocities of particles (left) and fluid (right) after time $t = 20$. $\varepsilon = 10^{-5}$. The gravity is considered.

In Figure 7(c), where $\varepsilon = 10^{-4}$, the particles are stopped immediately by the drag force when they enter the square domain and accumulate near the entrance. The streamline of particles and fluid are quite close to each other, except in the area close the entrance.

4.3.3 Simulation of Cavity Flow

Finally we apply our scheme on cavity flow. The cavity flow happens in a wide range of area, for example, the car sunroof and aircraft landing gear well.

We simulate the fluid flowing past an open cavity. Initially the cavity is full of rest fluid and the particle sediments are resting near the bottom corner of the cavity. The outside fluid flows past the opening of the cavity with a constant velocity, which drives the inside fluid circulating in the cavity. For simplicity we assume that the particle cannot escape the cavity, although our scheme can be easily generalized to the case when this escape happens.

We give the initial and boundary conditions corresponding to this description,

$$\begin{aligned} &n(0,\mathbf{x}) = 10^{-10} + \mathbf{1}_{0\le x\le 0.5, 0\le y\le 0.5},\\ &\mathbf{u}_p(0,\mathbf{x}) = 0,\\ &\mathbf{u}(0,\mathbf{x}) = 0. \end{aligned}$$

with

$$\mathbf{u}(t,\mathbf{x}) = \begin{pmatrix} 2 \\ 0 \end{pmatrix}, \quad \text{if } y = 1.$$

We need to modify (15) and (21) accordingly to incorporate this boundary condition. The Reynolds number is also incorporate into the incompressible Navier-Stokes system in the usual way

$$\begin{cases} \partial_t u + \nabla_x \cdot (u \otimes u) + \nabla_x p - \dfrac{1}{\mathrm{Re}} \Delta_x u = \dfrac{1}{\varepsilon} \kappa \displaystyle\int (v-u) f \,\mathrm{d}v, \\ \nabla_x \cdot u = 0. \end{cases} \tag{31}$$

We take $\varepsilon = 10^{-5}$ and neglect the gravity effect. The first simulation is performed with Reynolds number $\mathrm{Re} = 1$. Figure 8 shows the time evolution of particle density distribution until $t = 32$. Figure 9 shows the streamlines of the particles (left) and the fluid (right) at time $t = 32$. The particles move along the streamline of fluid and circulate in the cavity. Besides, noting that the maximum value of particle density is decreasing and the minimum value is increasing as time evolves, the particles are gradually spreading to the whole cavity.

Next we perform the simulation with a relatively large Reynolds number. The parameters in our simulation allow us to compute with Reynolds number up to $\mathrm{Re} = 400$ without trouble in stability. Larger Reynolds number, which requires smaller mesh size Δx for the sake of accuracy, is beyond the scope of this work.

Figure 10 shows the time evolution of particle density distribution for the same cavity problems with $\mathrm{Re} = 400$. The left bottom corner keeps more particles while the right bottom corner has very few. Figure 11 shows the streamlines of the particles (left) and the fluid (right) at time $t = 32$. A second circulation is formed in the corner.

Acknowledgements

This work started with a visit of Th. G. at the Math. Department of UW-Madison. Thanks are addressed to local brewers for unforgetable cheers. We are also gratefully indebted to Caterina Calgaro for useful advices.

Jian-Guo Liu is supported by NSF grant DMS-10-11738. Shi Jin is supported by NSF grant DMS-0608720 and NSF FRG grant DMS-0757285. Shi Jin is also supported by a Van Vleck Distinguished Research Prize and a Vilas Associate Award from the University of Wisconsin-Madison.

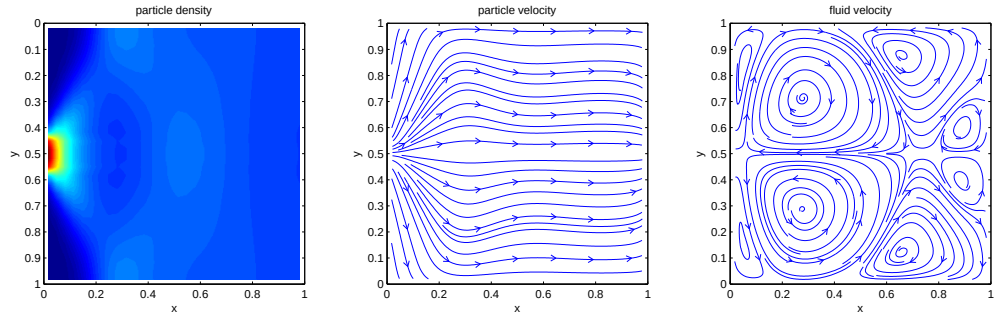

(a) $\varepsilon = 1$.

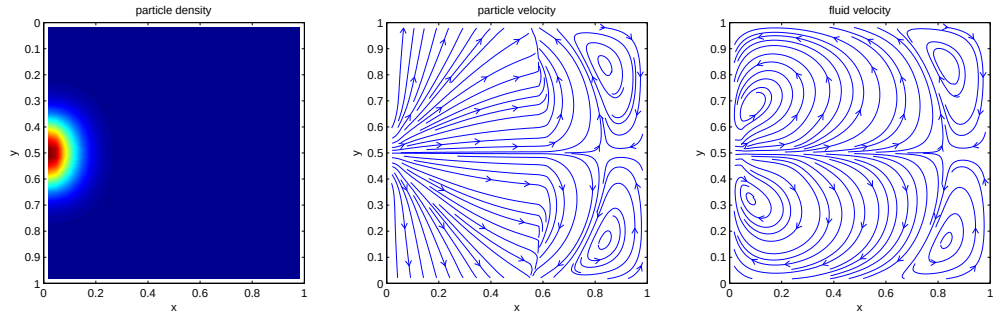

(b) $\varepsilon = 10^{-2}$.

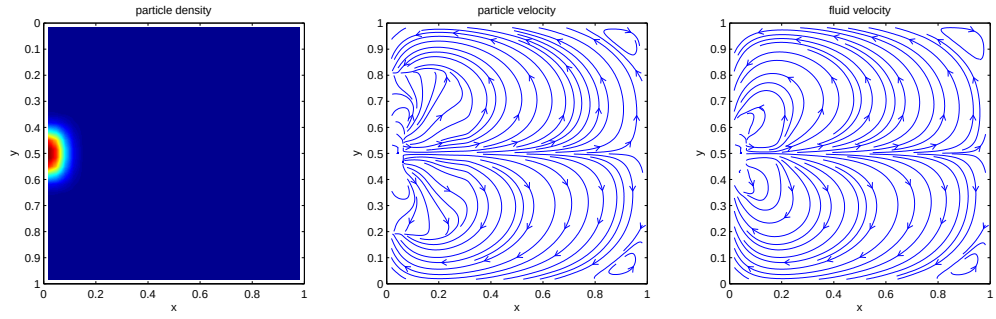

(c) $\varepsilon = 10^{-4}$.

Figure 7: The streamlines of velocities of particles (left) and fluid (right) after time $t = 0.5$ for the injecting problem. $\varepsilon = 1$. The gravity is considered.

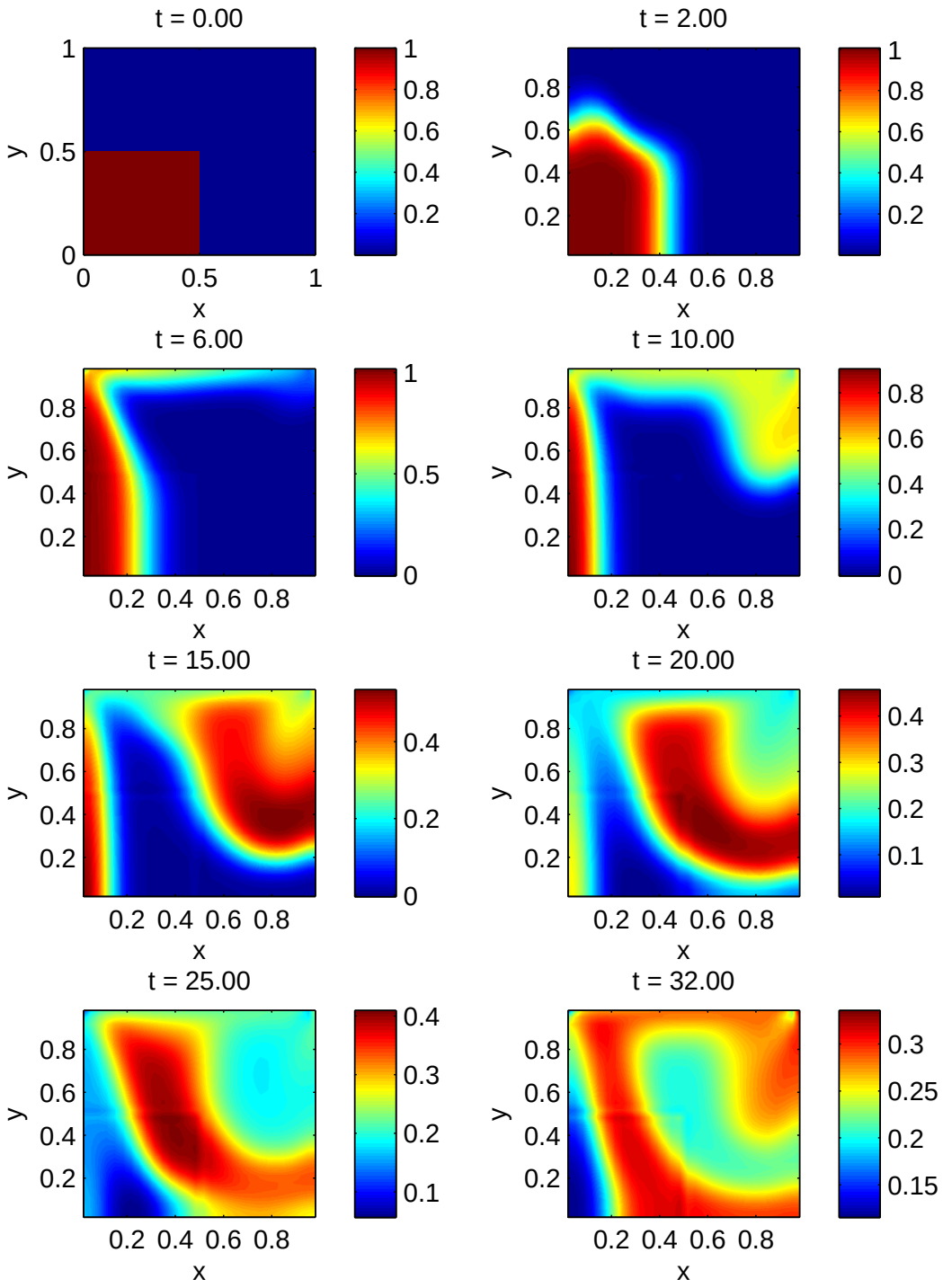

Figure 8: The time evolution of density of particle distribution in cavity flow, with Reynolds number $\mathrm{Re} = 1$. Here $\varepsilon = 10^{-5}$. The gravity is neglected.

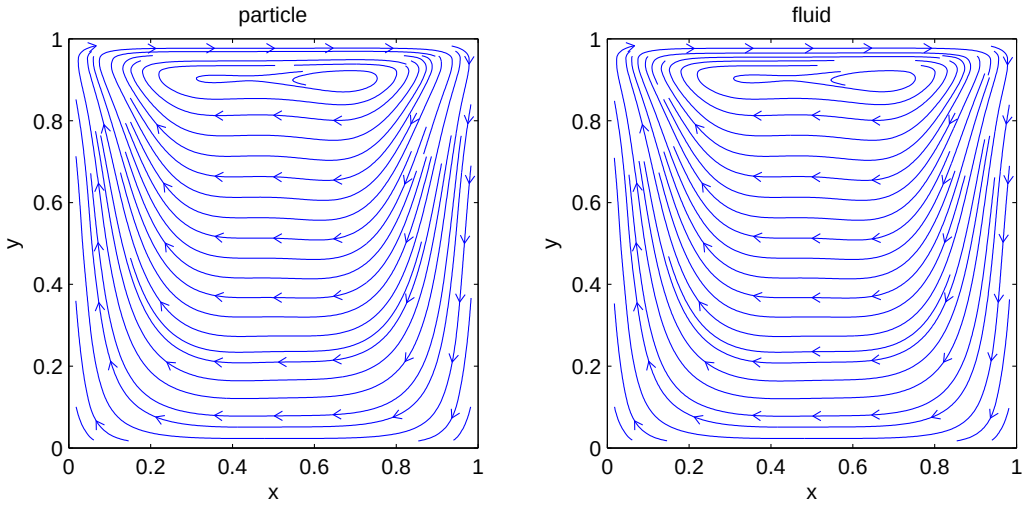

Figure 9: The streamlines of velocities of particles (left) and fluid (right) after time $t = 32$ in cavity flow, with Reynolds number $\mathrm{Re} = 1$. Here $\varepsilon = 10^{-5}$. The gravity is neglected.

References

[1] C. Baranger, G. Baudin, L. Boudin, B. Després, F. Lagoutière, F. Lapébie, and T. Takahashi. Liquid jet generation and break-up. In S. Cordier, T. Goudon, M. Gutnic, and E. Sonnendrucker, editors, *Numerical Methods for Hyperbolic and Kinetic Equations*, volume 7 of *IRMA Lectures in Mathematics and Theoretical Physics*. EMS Publ. House, 2005.

[2] C. Baranger, L. Boudin, Jabin P.-E., and S. Mancini. A modeling of biospray for the upper airways. *ESAIM:Proc*, 14:41–47, 2005.

[3] C. Baranger and L Desvillettes. Coupling Euler and Vlasov equations in the context of sprays: local smooth solutions. *Journal of Hyperbolic Differential Equations*, 3(1):1–26, 2006.

[4] J. Bell, P. Colella, and H. Glaz. A second-order projection method for the incompressible navier-stokes equations. *J. Comput. Phys.*, 85(2):257 – 283, 1989.

[5] S. Berres, R. Bürger, and E. M. Tory. Mathematical model and numerical simulation of the liquid fluidization of polydisperse solid particle mixtures. *Comput. Visual Sci.*, 6:67–74, 2004.

[6] L. Boudin, B. Boutin, B. Fornet, T. Goudon, P. Lafitte, F. Lagoutière, and B. Merlet. Fluid-particles flows: A thin spray model with energy exchanges. *ESAIM: Proc.*, 28:195–210, 2009.

[7] L. Boudin, L. Desvillettes, C. Grandmont, and A. Moussa. Global existence of solutions for the coupled Vlasov and Navier-Stokes equations. *Differential and Integral Equations*, 22(11–12), 2009.

[8] B. Boutin and P. Lafitte. Splitting schemes for fluid-particles flows with energy exchanges. Work in progress.

[9] R. Caflisch and G. Papanicolaou. Dynamic theory of suspensions with Brownian effects. *SIAM J. Appl. Math.*, 43:885–906, 1983.

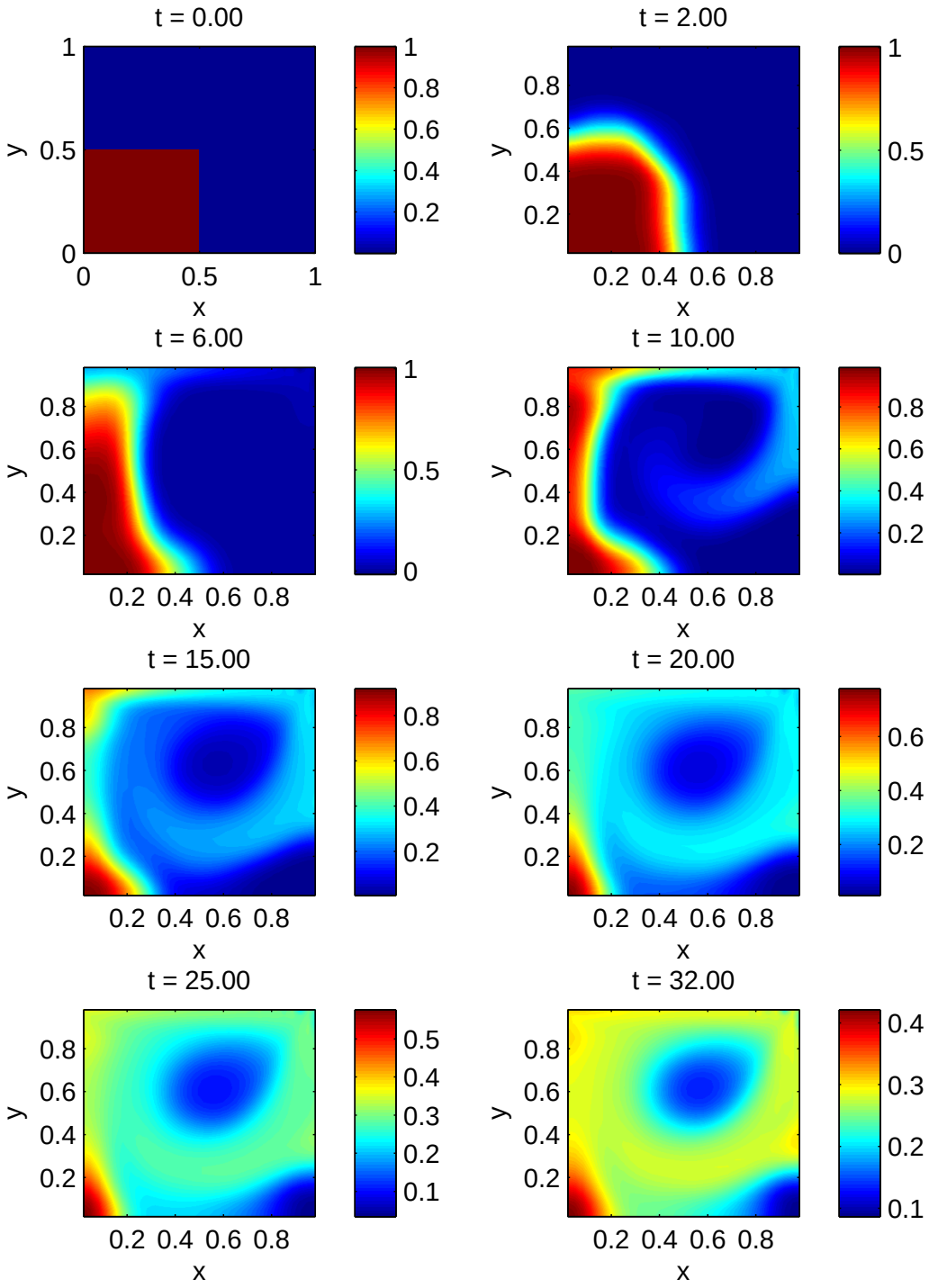

Figure 10: The time evolution of density of particle distribution in cavity flow, with Reynolds number Re = 400. Here $\varepsilon = 10^{-5}$. The gravity is neglected.

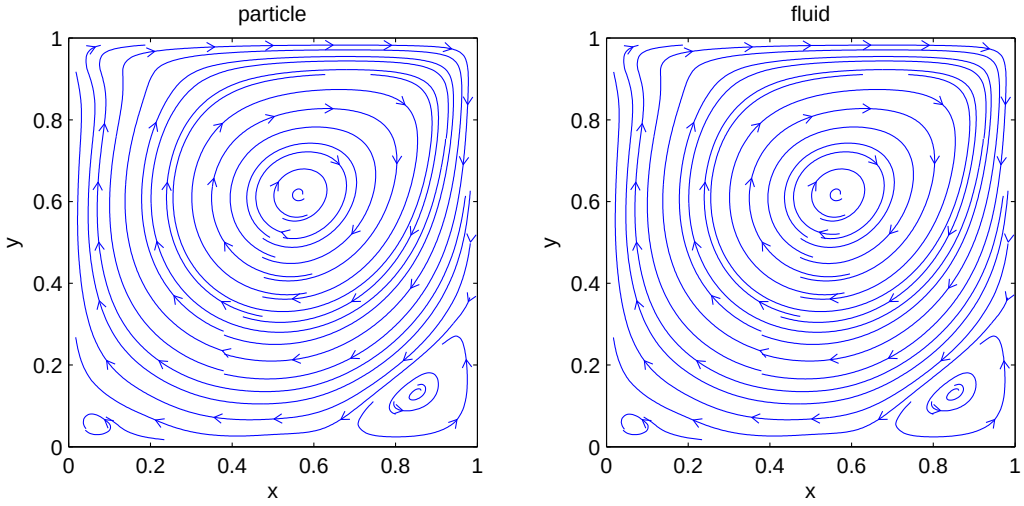

Figure 11: The streamlines of velocities of particles (left) and fluid (right) after time $t = 32$ in cavity flow, with Reynolds number $\mathrm{Re} = 400$. Here $\varepsilon = 10^{-5}$. The gravity is neglected.

[10] J.-A. Carrillo, R. Duan, and A. Moussa. Global classical solutions close to equilibrium to the Vlasov-Euler-Fokker-Planck system. *Kinetic and Related Models*, 4(1):227–258, 2011.

[11] J. A. Carrillo and T. Goudon. Stability and asymptotics analysis of a fluid-particles interaction model. *Comm. PDE*, 31:1349–1379, 2006.

[12] J. A Carrillo, T. Goudon, and P. Lafitte. Simulation of fluid & particles flows: Asymptotic preserving schemes for bubbling and flowing regimes. *J. Comput. Phys.*, 227(16):7929–7951, 2008.

[13] J.-A. Carrillo, T. Karpery, and K. Trivisa. On the dynamics of a fluid-particle interaction model: The bubbling regime. Technical report, UABarcelona, 2010. Preprint.

[14] A. Chorin. The numerical solution of the Navier-Stokes equations for an incompressible fluid. *Bull. Amer. Math. Soc.*, 73:pp. 928–931, 1967.

[15] A. Chorin. Numerical solution of the Navier-Stokes equations. *Math. Comp.*, 22(104):745–762, 1968.

[16] A. Chorin. On the convergence of discrete approximations to the Navier-Stokes equations. *Math. Comp.*, 23(106):341–353, 1969.

[17] M. De Luca. *Contribution à la modélisation de la pulvérisation dun liquide phytosanitaire en vue de réduire les pollutions*. PhD thesis, Univ. Aix–Marseille 2, 2007.

[18] L. Desvillettes. Some new results of existence for the theory of sprays. `http://www.newton.ac.uk/programmes/KIT/seminars/090710001.html`, 2010. Workshop "Fluid-Kinetic Modelling in Biology, Physics and Engineering", Isaac Newton Institute for Mathematical Sciences, Programme on PDEs in Kinetic Theories.

[19] L. Desvillettes, F. Golse, and V. Ricci. The mean-field limit for solid particles in a Navier-Stokes flow. *J. Stat. Phys.*, 131(5):941–967, 2008.

[20] A. Einstein. On the motion of small particles suspended in liquids at rest required by the molecular-kinetic theory of heat. *Ann. Physik*, 17:549–560, 1905.

[21] A. Einstein. Eine neue bestimmung der moleküldimensionen. *Ann. Physik*, 19:289–306, 1906. Doctoral dissertation, Zurich, 1905.

[22] T. Elperin, N. Kleeorin, M.A. Liberman, V.S. L'vov, A. Pomyalov, and I Rogachevskii. Clustering of fuel droplets and quality of spray in Diesel engines. 2003. `http://arxiv.org/nlin.CD/0305017v1`.

[23] J. Filbet and S. Jin. A class of asymptotic–preserving schemes for kinetic equations and related problems with stiff sources. *J. Comp. Phys.*, 229(20):7625–7648, 2010.

[24] V. S. Galkin and S. V. Rusakov. Kinetic Fokker–Planck equation for free-molecular, thermally nonequilibrium Brownian particles in an inhomogeneous gas. *Fluid Dynamics*, 42:330–334, 2007. Originally published in Izvestiya Rossiiskoi Akademii Nauk, Mekhanika Zhidkosti i Gaza, 2007, Vol. 42, No. 2, pp. 204–208 (in Russian).

[25] T. Goudon, P.-E. Jabin, and A. Vasseur. Hydrodynamic limit for the Vlasov-Navier-Stokes equations. I. Light particles regime. *Indiana Univ. Math. J.*, 53(6):1495–1515, 2004.

[26] T. Goudon, P.-E. Jabin, and A. Vasseur. Hydrodynamic limit for the Vlasov-Navier-Stokes equations. II. Fine particles regime. *Indiana Univ. Math. J.*, 53(6):1517–1536, 2004.

[27] T. Goudon, S. Jin, and B. Yan. Simulation of fluid–particles flows: Heavy particles, flowing regime and AP–schemes. *Comm. Math. Sci.*, to appear.

[28] T. Goudon, A. Moussa, L. He, and P. Zhang. The Navier–Stokes–Vlasov–Fokker–Planck system near equilibrium. *SIAM J. Math. Anal.*, 42(5):2177–2202, 2010.

[29] K. Hamdache. Global existence and large time behaviour of solutions for the Vlasov-Stokes equations. *Japan J. Indust. Appl. Math.*, 15:51–74, 1998.

[30] M. Ishii and T. Hibiki. *Thermo–fluid dynamics of two–phase flows.* Springer, 2011. 2nd edition.

[31] S. Jin. Efficient asymptotic–preserving (AP) schemes for some multiscale kinetic equations. *SIAM J. Sci. Comput.*, 21(2):441–454, 1999.

[32] S. Jin. Asymptotic preserving (AP) schemes for multiscale kinetic and hyperbolic equations: a review. *Lecture Notes for Summer School on "Methods and Models of Kinetic Theory" (M&MKT), Porto Ercole (Grosseto, Italy), June 2010. Rivista di Matematica della UniversitÃ di Parma*, to appear.

[33] S. Jin and B. Yan. An AP scheme for the Fokker–Planck–Landau equation. *J. Comput. Phys.*, to appear.

[34] J. Kim and P. Moin. Application of a fractional-step method to incompressible Navier-Stokes equations. *J. Comput. Phys.*, 59(2):308 – 323, 1985.

[35] G. Lavergne. *Modélisation de l'écoulement multiphasique dans le propulseur à poudre P230 d'Ariane 5*, 2004. Lecture Notes of the School of the Groupement Français de Combustion, Ile d'Oléron.

[36] J. Mathiaud. *Etude de systèmes de type gaz-particules.* PhD thesis, ENS Cachan, 2006.

[37] A. Mellet and A. Vasseur. Global weak solutions for a Vlasov-Fokker-Planck/Navier-Stokes system of equations. *Math. Mod. Meth. Appl. Sci*, 17(7):1039–1063, 2007.

[38] A. Mellet and A. Vasseur. Asymptotic analysis for a Vlasov–Fokker–Planck/compressible Navier–Stokes system of equations. *Comm. Math. Phys.*, 281(3):573–596, 2008.

[39] A. Moussa. *Etude mathématique et numérique du transport d'aérosols dans le poumon humain.* PhD thesis, ENS Cachan, 2009.

[40] P. J. O'Rourke. *Collective Drop Effects on Vaporizing Liquid Sprays.* PhD thesis, Princeton Univ., 1981. Available as Technical Report #87545 Los Alamos National Laboratory.

[41] N. A. Patankar and D. D. Joseph. Lagrangian numerical simulation of particulate flows. *Int. J. Multiphase Flow*, 27:1685–1706, 2001.

[42] N. A. Patankar and D. D. Joseph. Modeling and numerical simulation of particulate flows by the Eulerian–Lagrangian approach. *Int. J. Multiphase Flow*, 27:1659–1684, 2001.

[43] A. Quarteroni, R. Sacco, and F. Saleri. *Numerical Mathematics.* Springer, second edition, 2007.

[44] Y. Sina, P. Stopford, M. Edwards, and S. Watkins. CFD modelling of fire suppression by water spray: Sensitivity and validation for a pool fire in a room. In *Eighth International IBPSA Conference Eindhoven, Netherlands*, 2003.

[45] D. M. Snider, P. J. O'Rourke, and M. J. Andrews. Sediment flow in inclined vessels calculated using a multiphase particle-in-cell model for dense particle flows. *Int. J. Multiphase Flow*, 24:1359–1382, 1998.

[46] B. Sportisse. *Modélisation et simulation de la pollution atmosphérique.* PhD thesis, Université Pierre et Marie Curie, 2007. Habilitation à Diriger les Recherches, Sciences de l'Univers.

[47] R. Temam. Sur l'approximation de la solution des equations de Navier-Stokes par la méthode des fractionnarires ii. *Arch. Rational Mech. Anal.*, 33:377–385, 1969.

[48] I. Vinkovic. *Dispersion et mélange turbulents de particules solides et de gouttelettes par une simulation des grandes échelles et une modélisation stochastique lagrangienne. Application à la pollution de l'atmosphère.* PhD thesis, Ecole Centrale de Lyon, 2005.

[49] F. A. Williams. *Combustion theory.* Benjamin Cummings Publ., 1985. (2nd edition).